JOURNAL OF MATERIALS SCIENCE 33 (1998) 1023–1030

Interdiffusion reaction in the PZT/PNN functionally gradient piezoelectric ceramic materials

XINHUA ZHU*
Department of Physics and National Laboratory of Solid State Microstructures, Nanjing University, Nanjing 210093, People's Republic of China

JIE XU, ZHONGYAN MENG
School of Materials Science & Engineering, Shanghai University (Jiading Campus), Shanghai 201800, People's Republic of China

The interfacial diffusion reaction between lead zirconate titanate (PZT) and lead nickel niobate ($PbNi_{1/3}Nb_{2/3}O_3$:PNN) phases in the PZT/PNN functionally gradient piezoelectric ceramics were investigated as a function of the diffusion temperature and time, respectively. The ionic composition distribution profiles in the interdiffusion region were examined by electron probe microbeam analysis (EPMA). Based on a diffusion model of the overlapped diffusion solution from thin slab, the numerical simulation for the ionic composition distribution was carried out by computer, which was in agreement with the EPMA result. The diffusion coefficients for the Ni^{2+}, Nb^{5+}, Ti^{4+} and Zr^{4+} ions were determined, which were 33.8, 22.6, 10.8 and $9.9 \times 10^{-12}\,m^2\,s^{-1}$, respectively. The apparent activation energies for these ions were 94.4, 171.7, 257.5 and 325.8 $kJ\,mol^{-1}$, respectively. The differences in the ionic diffusion coefficients and apparent activation energies were discussed from the viewpoint of the crystal chemistry.

1. Introduction

Recent advances in technology, particularly in micromechanics, require microscale actuators that can be used in severe environments with high reliability. The main shortcomings of the usual piezoelectric bimorphs are the low reliability and poor interfacial bonding conditions resulting from the fact that the bonding agent (usually epoxy resin) may crack and spall off at low temperature, and creep at high temperature [1]. After the concept of the functionally gradient materials (FGM) was proposed and extended into the piezoelectric ceramic materials, a FGM piezoelectric actuator was developed to overcome the performance limitations of the usual piezoelectric bimorphs. Within the FGM piezoelectric actuator, the bonding agent was replaced by a graded interdiffusion layer, in which the compositional and microstructural gradients over the macroscopic distance were tailored for the functional requirements of the electric properties [2]. The formation and compositional variations of the interdiffusion layer play an important part in affecting the interfacial bonding conditions and the electric field-induced displacement characteristics of a FGM piezoelectric actuator. It is necessary to investigate the formation kinetics of the interdiffusion layer and the interdiffusion reaction in the FGM piezoelectric ceramic actuator before the proceeding conditions of the FGM actuators are optimized.

In this paper, the interdiffusion results of the diffusion couple in the lead zirconate titanate/lead nickel niobate (PZT/PNN) FGM piezoelectric ceramics examined by electron probe microbeam analysis (EPMA) are presented. The ionic composition distributions were numerically simulated by computer, and the results were compared with that of the EPMA experiment. The diffusion coefficients and apparent activation energies for the diffusion ions were determined.

2. Experimental procedure

For preparation of the diffusion couple, the calcined powders of $Pb(Ni_{1/3}Nb_{2/3})O_3$ and $Pb(Zr, Ti)O_3$ were first made by calcining all the constituent metal oxide powders at 860 °C for 3 h. Considering the difference in the sintering contraction between the PNN and PZT phases in the PZT/PNN diffusion couple, in this study, we have chosen six compositions to construct three diffusion couples, which are presented in Table I. The powders of A and B compositions were obtained by mixing the calcined powders of PNN and PZT according to the chemical formulas given in Table I.

* Author to whom correspondence should be addressed.

An appropriate amount of polyvinyl alcohol (PVA) binder was added to the dried powders of A and B compositions, respectively, which were then granulated for fabrication of the A–B diffusion couple. The powder of A or B was first cold-pressed into discs (20 mm dia, 4 mm thickness) under a pressure of 30 MPa, then the powder of B or A was laminated into the mould and cold pressed again under 30 MPa pressure. The diffusion couple was constructed with 8 mm thickness and sintered at temperature ranges from 1150 to 1280 °C in air for different times. The annealed couples were cut perpendicular to the interdiffusion layer's direction and polished on both sides for EPMA analysis. The composition distributions in the cross-section of the interdiffusion layers were examined by EPMA, from which the width of the interdiffusion layer was determined. The EPMA experiment was performed in the EPMA-8750QH (Daojin Corp., Japan), operated at 20 kV with 10 μm step width.

TABLE I Compositions used in this study and the constructed diffusion couples

Compositions (mol)	Diffusion couples
A: 0.1PNN–0.9 $(Zr_{0.6}Ti_{0.4})O_3$ B: 0.9PNN–0.1 $(Zr_{0.6}Ti_{0.4})O_3$	A–B
C: 0.2PNN–0.8 $(Zr_{0.6}Ti_{0.4})O_3$ D: 0.8PNN–0.2 $(Zr_{0.6}Ti_{0.4})O_3$	C–D
E: 0.3PNN–0.7 $(Zr_{0.6}Ti_{0.4})O_3$ F: 0.7PNN–0.3 $(Zr_{0.6}Ti_{0.4})O_3$	E–F

3. Results and discussion

3.1. Characteristic X-ray intensity distribution

The typical distribution of the characteristic X-ray intensity for the diffusion ions versus the measured positions (diffusion conditions: 1250 °C/2 h, C–D diffusion couple) are shown in Fig. 1. It is shown that in Fig. 1a there are two plateaus at both sides and a graded region in the middle of the scanned distance. The higher plateau represents the higher initial content of Nb in composition D, and the lower one for the smaller initial content of Nb in composition C. The graded part means the interdiffusion layer, in which the compositions vary gradually. Similar phenomena are also observed for other diffusion ions, as shown in Fig. 1b–d.

3.2. Compositional distribution

The compositional distribution profiles for the diffusion ions of the A–B, C–D and E–F diffusion couples examined by EPMA across the section of the interdiffusion region formed at different diffusion conditions are shown in Figs 2–7. With increasing the diffusion temperature or time, the curves of the compositional distribution profiles of the C–D and E–F diffusion couples, as illustrated in Figs 4–7, are still composed of two plateaus at both sides and a graded part in the middle of the scanned regions. However, the graded part becomes much broader and the compositional distribution seems to be much smoother. *Such a phenomenon does not occur for the A–B diffusion couple. The reason is that with high phase compositional gradi-*

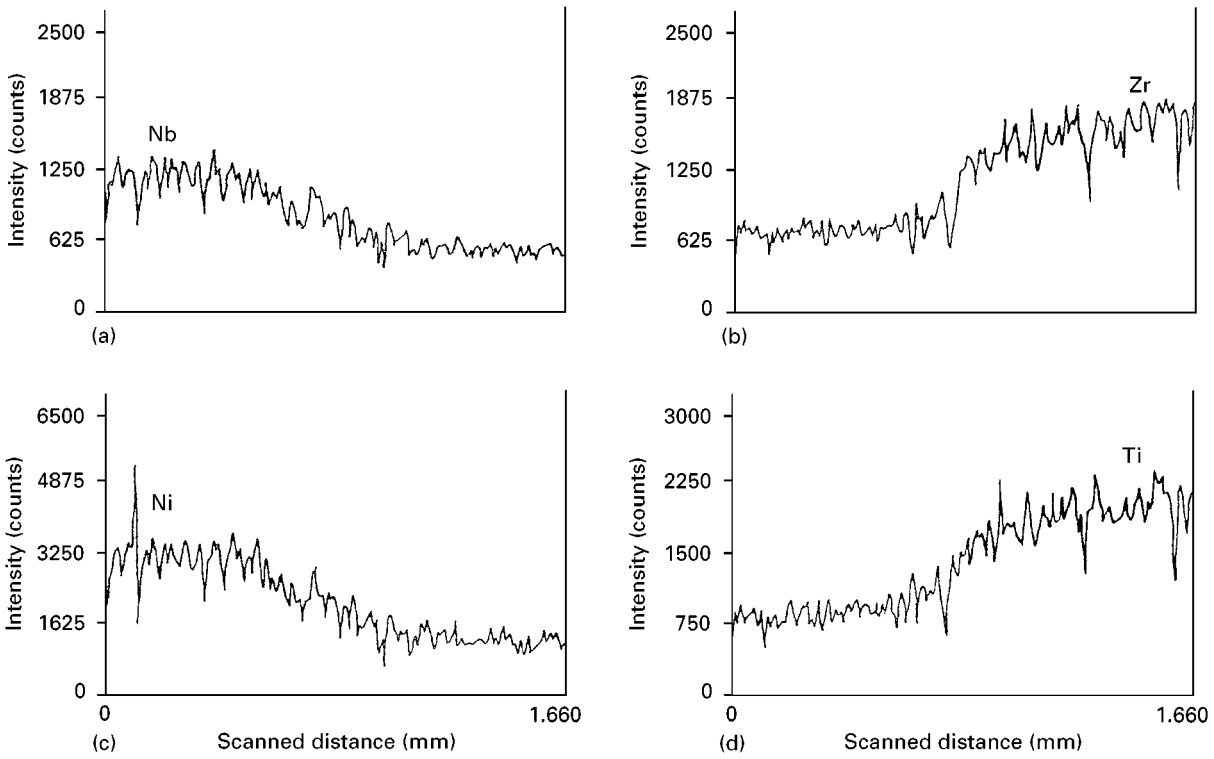

Figure 1 Typical distribution curves of the characteristic X-ray intensities for different diffusion ions versus the scanned distances. Diffusion conditions: 1250 °C/2 h, C–D diffusion couple. (a) Nb; (b) Zr; (c) Ni; (d) Ti.

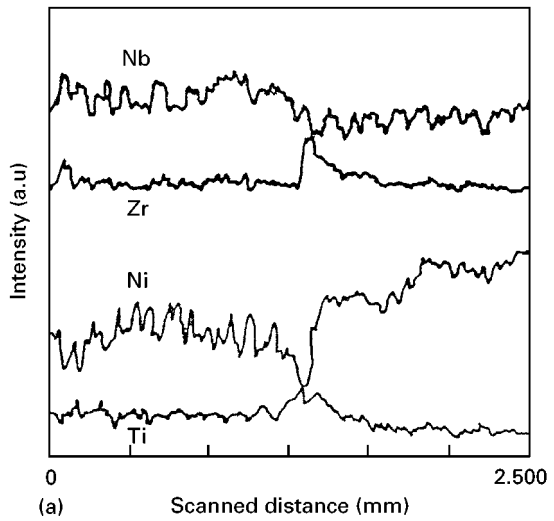

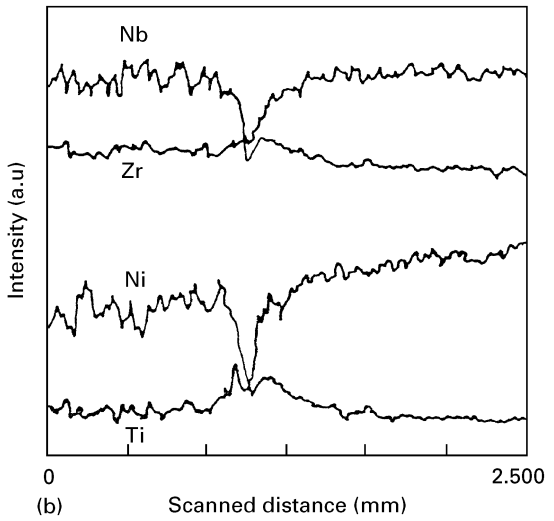

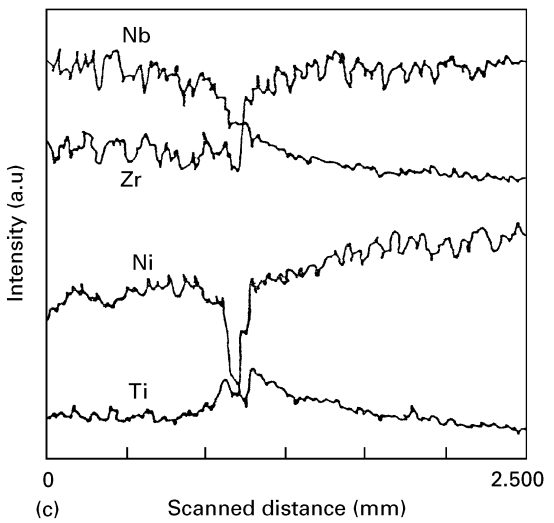

Figure 2 Compositional distribution profiles of the diffusion ions for the A–B diffusion couple at 1230 °C for (a) 120 min, (b) 240 min and (c) 360 min.

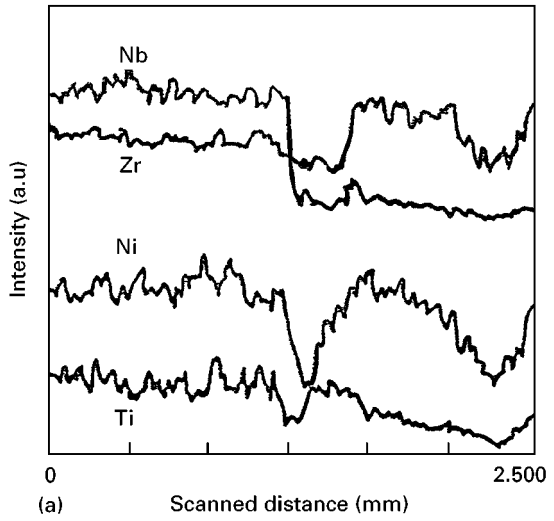

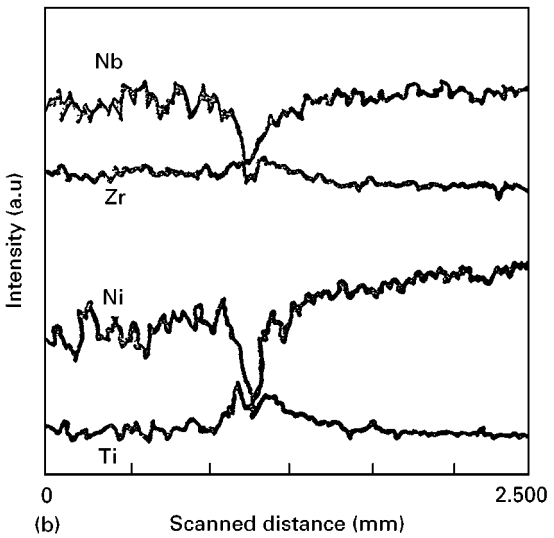

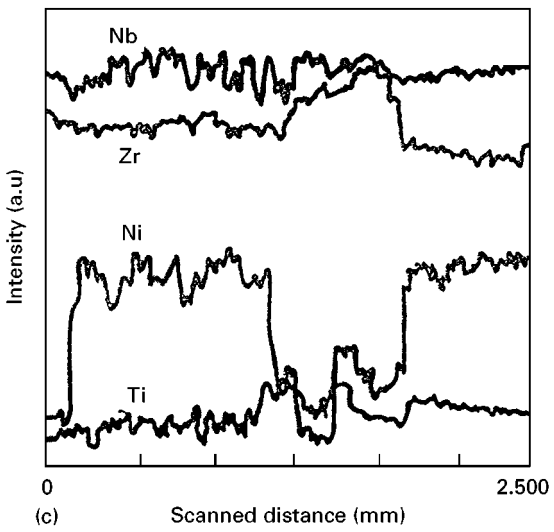

Figure 3 Compositional distribution profiles of the diffusion ions for the A–B diffusion couple at (a) 1200 °C, (b) 1230 °C and (c) 1250 °C for 240 min.

ent in the A–B diffusion couple (seen in Table I), the compatibility between the PZT and PNN phases become poor because of their different sintering contractions, and at higher diffusion temperature the tendency to crack and spall is stronger than that of the interdiffusion reaction, which results in a poor interdiffusion layer and low interfacial diffusion bonding. This has been identified by scanning electron microscopy (SEM) observations. Therefore, with increasing the diffusion temperature the curves of the compositional profiles of the A–B diffusion couple become sharper instead of smoother in the middle of the scanned regions, as shown in Figs 3a–c because of the stronger tendency to crack and spall. Fig. 8 demonstrates the ionic compositional

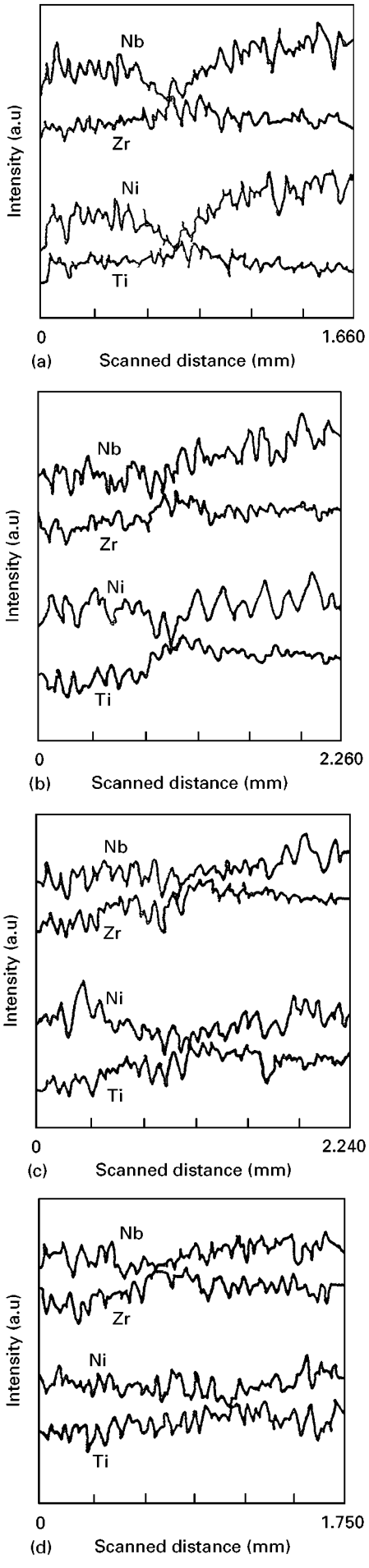

Figure 4 Compositional distribution profiles of the diffusion ions for the C–D diffusion couple at 1250 °C for (a) 120 min, (b) 240 min, (c) 360 min and (d) 480 min.

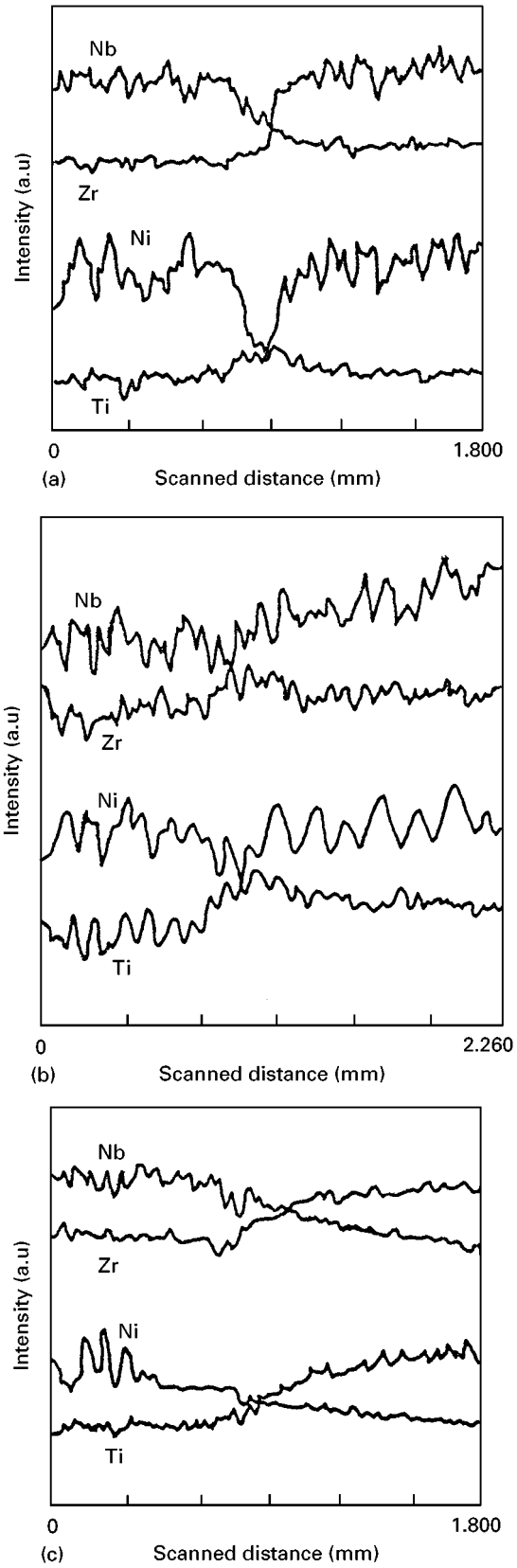

Figure 5 Compositional distribution profiles of the diffusion ions for the C–D diffusion couple at (a) 1200 °C, (b) 1250 °C and (c) 1280 °C for 240 min.

distribution profiles of the different diffusion couples under the same diffusion conditions. The higher phase compositional gradients in the diffusion couple, the higher driving force for diffusion reaction and the more clear graded composition distributions should be appeared. However, the graded variation in the

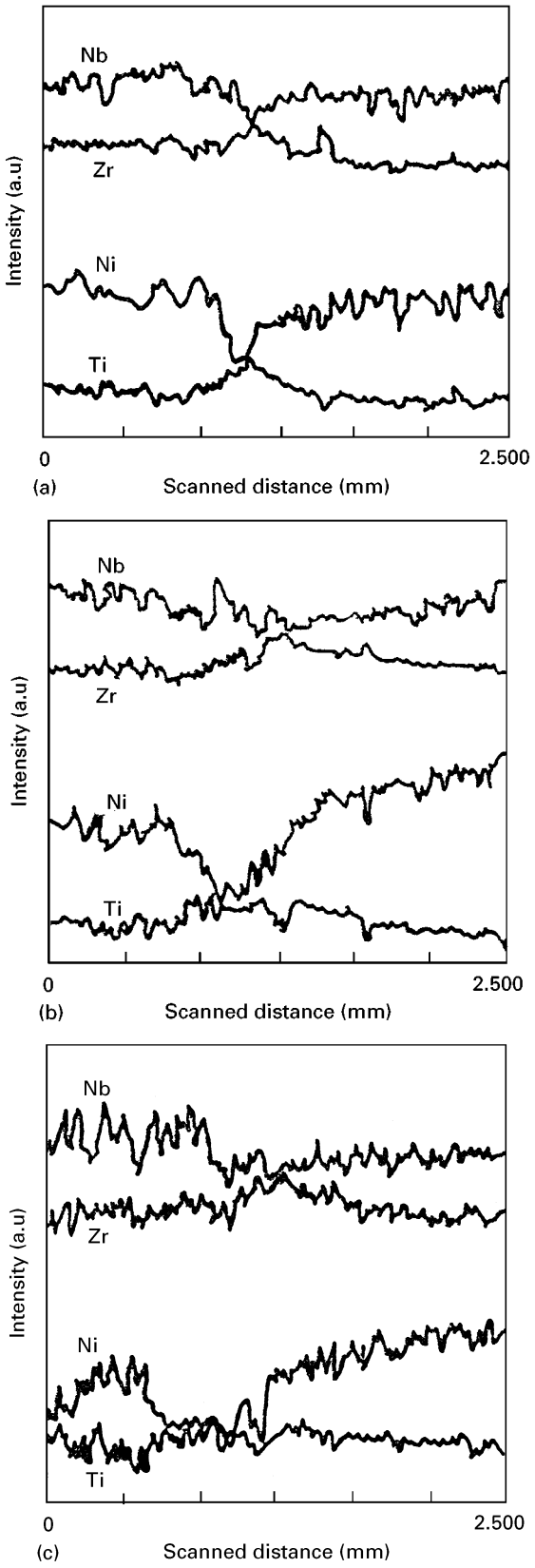

Figure 6 Compositional distribution profiles of the diffusion ions for the E–F diffusion couple at 1250 °C for (a) 120 min, (b) 240 min and (c) 360 min.

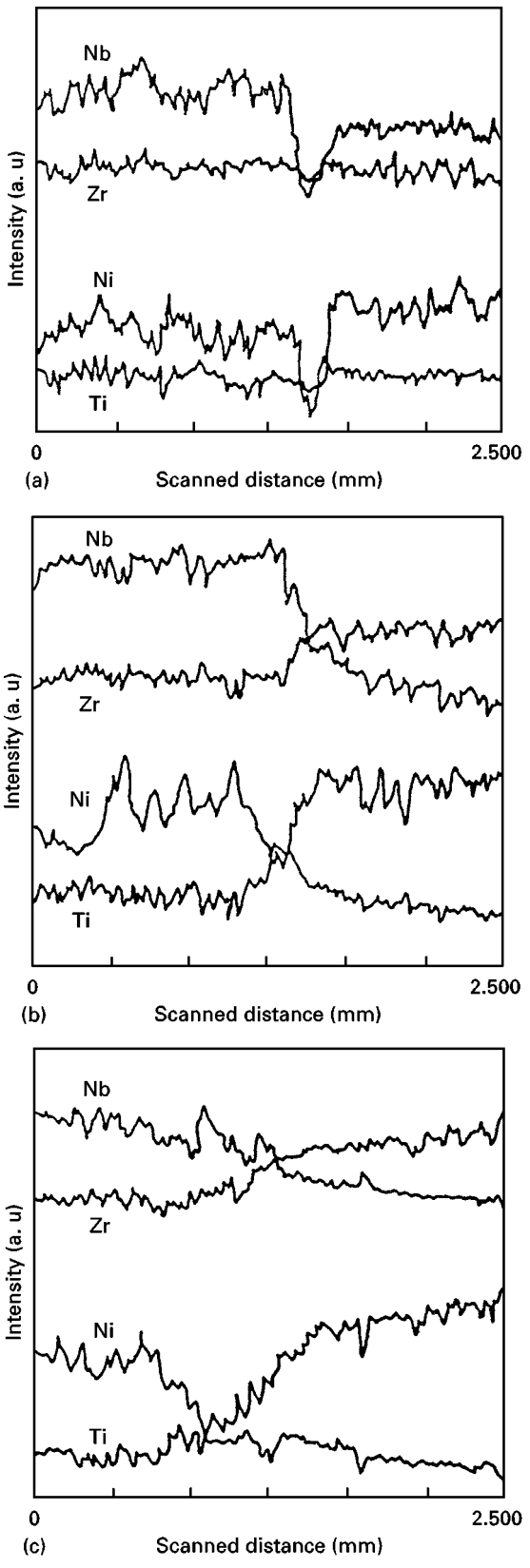

Figure 7 Compositional distribution profiles of the diffusion ions for the E–F diffusion couple at (a) 1200 °C, (b) 1230 °C and (c) 1250 °C for 240 min.

compositional distribution shown in Fig. 8 is not apparent. *The reason is the same as that for the A–B diffusion couple.* Attention should be paid to the compatibilities of the selected compositions for constructing the diffusion couples in the PZT/PNN piezoelectric ceramic system.

3.3. Interdiffusion layer formation

The width of the interdiffusion layer can be obtained by measuring the width of the graded part of the compositional distribution. Fig. 9 shows the square of the width of interdiffusion layer d^2 formed at 1250 °C for C–D diffusion couple versus the time t. As shown

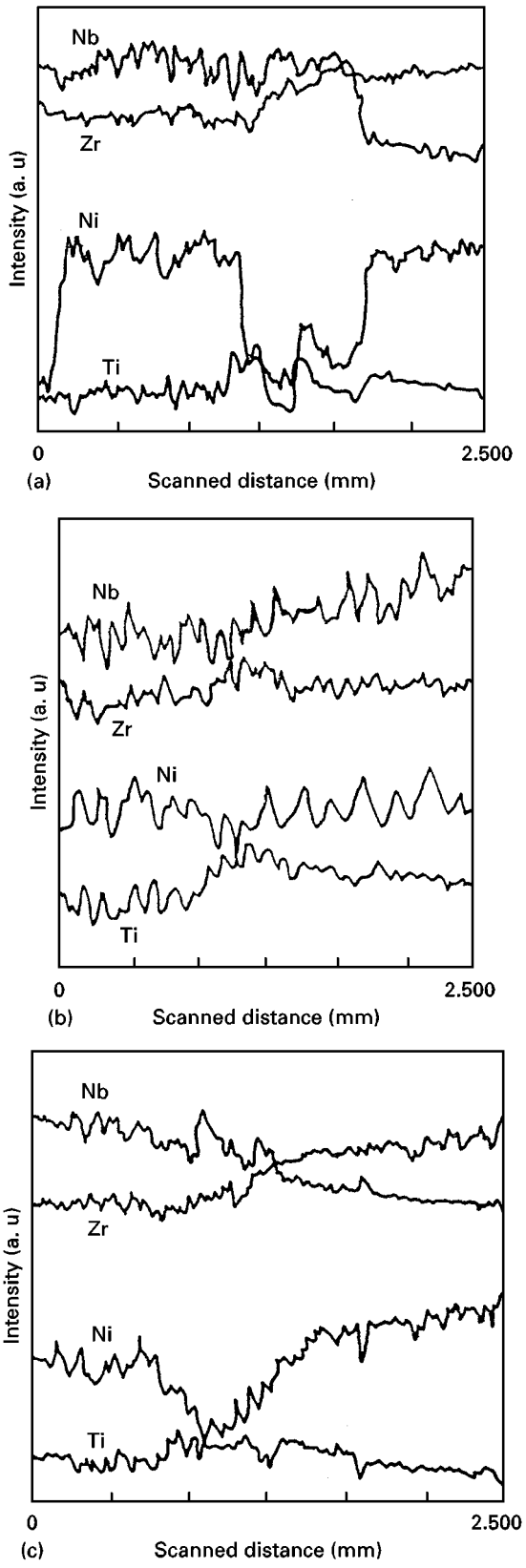

Figure 8 Compositional distribution profiles of the diffusion ions for different diffusion couples at the same diffusion conditions; (a) A–B, (b) C–D and (c) E–F diffusion couples.

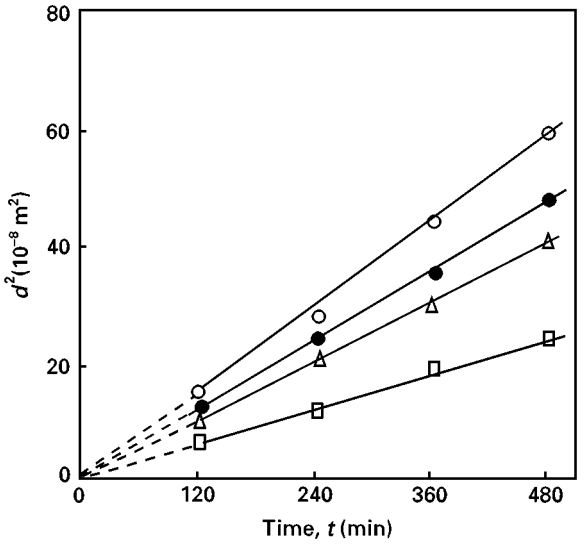

Figure 9 Square of the width of the interdiffusion layer formed at 1250 °C in C–D diffusion couple as a function of the time. (○) Ni^{2+}, (●) Nb^{5+}, (▲) Ti^{4+} and (□) Zr^{4+}.

in Fig. 9, the interdiffusion layer growth follows the parabolic growth law [3]

$$d^2 = kt \tag{1}$$

where d denotes the width of the interdiffusion layer, k is parabolic growth rate constant which has the dimension of the diffusivity, and t the time. The linear relationship between d^2 and t observed in Fig. 9 strongly suggests that the formation of the interdiffusion layer is controlled by the ionic diffusion. Because the curves are originated at the (0, 0) coordinate, it can be concluded that the interdiffusion occurs immediately without an incubation time at the investigated temperature range. The measured parabolic growth rate constants at a temperature of 1250 °C for Ni^{2+}, Nb^{5+}, Ti^{4+} and Zr^{4+} ions are 21.3, 17.5, 15.0 and $9.3 \times 10^{-12}\ m^2\ s^{-1}$, respectively. That means the magnitude of the diffusion coefficients for Ni^{2+}, Nb^{5+}, Ti^{4+} and Zr^{4+} ions can be ordered as $D_{Ni^{2+}} > D_{Nb^{5+}} > D_{Ti^{4+}} > D_{Zr^{4+}}$, which is interpreted as the effects of ionic radii and valence. The Pauling ionic sizes for Ni^{2+}, Nb^{5+}, Ti^{4+} and Zr^{4+} ions are 0.069, 0.07, 0.068 and 0.08 nm, respectively. The diffusing for Zr^{4+} ions from the PZT phase into the PNN phase substituting the Ni^{2+} and/or Nb^{5+} ions is restrained from the high lattice deformation resulted from the large mismatch at the ionic size. The reverse condition occurs for Ti^{4+} ions because of the almost identical ionic sizes between Ti^{4+} and Ni^{2+} or Nb^{5+} ions. The reason why the diffusion coefficient for Ni^{2+} ion is higher than that of Nb^{5+} ion is due to their different electrostatic energies within the oxygen octahedra. It seems that the reason for $D_{Nb^{5+}} > D_{Ti^{4+}}$ is not readily apparent. One possible explanation may be their different Dietzel field strengths. The Dietzel field strength is given as Z/r^2, where Z is the ionic valence, r is the distance between the ion and oxygen within the oxygen octahedra. The Dietzel field strength for Nb^{5+} ion is 1.13, and 0.92 for Ti^{4+} ion. The higher Dietzel field strength the cation has, the more polarizability the cation possesses. The cations with high polarizabilities can make their surrounding ions polarized and deformed, which can reduce the blocking effect presented at the diffusion path and make the ionic diffusion become relatively easier. To obtain the activation energy E_a for the rate-controlling process, one

can use an Arrhenius type relationship

$$k = A \exp(-E_a/RT) \quad (2)$$

where A is a pre-exponential constant, R and T denote the gas constant and absolute temperature, respectively. A typical Arrhenius plot for Ti^{4+} ion constructed as the logarithm of parabolic growth rate ($\log k$) versus $1/T$, is shown in Fig. 10. It is noticed that a linear relationship exists and the activation energy for Ti^{4+} ion is determined from its slope to be 257.5 kJ mol^{-1}. Similarly, the activation energies for other diffusion ions can be obtained, which are presented in Table II.

3.4. Numerical simulation for compositional distribution

Considering the width of the interdiffusion layer is much smaller than that of each semi-diffusion couple, the ionic interdiffusion in the couple could be regarded as the interdiffusion in a pair of semi-infinite solids. The ionic diffusion follows Fick's second law, which is expressed as

$$\frac{\partial c(x,t)}{\partial t} = \frac{\partial}{\partial x}\left(D\frac{\partial c(x,t)}{\partial x}\right) \quad (3)$$

If the diffusion coefficient D is independent of the position, Equation 3 simplifies to

$$\frac{\partial c(x,t)}{\partial t} = D\frac{\partial^2 c(x,t)}{\partial x^2} \quad (4)$$

It is assumed that the initial concentration distribution is simply stated as

$$\begin{aligned} &c = c_0, \quad \text{at } x < 0, \quad \text{for } t = 0 \\ &c = c', \quad \text{at } x > 0, \quad \text{for } t = 0 \end{aligned} \qquad (c' > c_0) \quad (5)$$

The solution to Equation 4 can be yielded by the application of the above boundary conditions in the following manner: imagine the region of $x > 0$ is composed of n slices, each with $\Delta\lambda$ thickness and unit cross-sectional area. For each slice, the diffusion solution can be given by thin film solution. If the interactions between the adjacent slices during the diffusion process are neglected, the actual diffusion solution can be obtained by the overlapping the diffusion solution of each thin slice, which is expressed as [4]

$$c(x,t) = c_0 + \frac{c' - c_0}{2(\pi Dt)^{\frac{1}{2}}}\sum_{i=1}^{n}\Delta\lambda_i \exp\left[-\frac{(x-\lambda_i)^2}{4Dt}\right] \quad (6)$$

where $c(x,t)$ represents the concentration, λ_i is the distance from the centre of the ith slice to the plane of $x = 0$. When the number of the slices n goes to infinity, $\Delta\lambda_i \to 0$, Equation 6 can be written by an integral form, that is

$$c(x,t) = c_0 + \frac{c' - c_0}{2(\pi Dt)^{\frac{1}{2}}}\int_0^{\infty}\exp\left[-\frac{(x-\lambda_i)^2}{4Dt}\right]d\lambda \quad (7)$$

Setting $x - \lambda/2(Dt)^{\frac{1}{2}} = \eta$ and introducing the Gaussian error function

$$erf(z) = \frac{2}{\pi^{\frac{1}{2}}}\int_0^z \exp(-\eta^2)d\eta \quad (8)$$

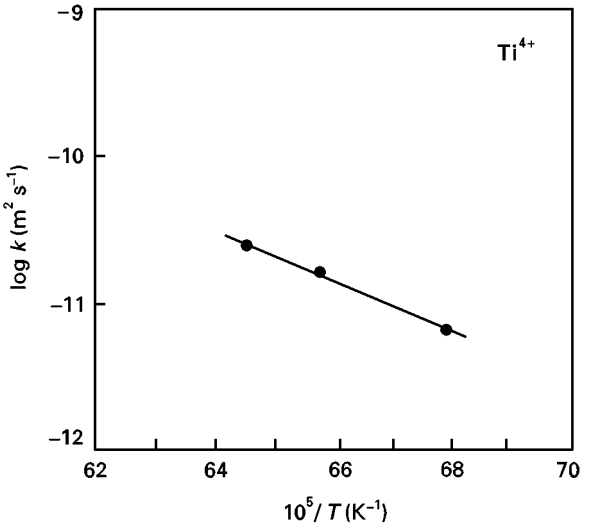

Figure 10 Typical logarithm of the parabolic growth rate constant ($\log k$) for Ti^{4+} ion versus the reciprocal temperature ($1/T$).

TABLE II Properties of the diffusion ions

Diffusion ions	Growth rate constant[a] k (10^{-12} m^2 s^{-1})	Activation energy E_a (kJ mol^{-1})	Diffusion coefficient* D (10^{-12} m^2 s^{-1})
Ni^{2+}	21.3	94.4	33.8
Nb^{5+}	17.5	171.7	22.6
Ti^{4+}	15.0	257.5	10.8
Zr^{4+}	9.3	325.8	9.9

[a]Diffusion conditions 1250 °C.

Equation 7 can be rewritten as

$$c(x,t) = c_0 + \frac{c' - c_0}{2}\left[1 + erf\left(\frac{x}{2(Dt)^{\frac{1}{2}}}\right)\right] \quad (9)$$

The normalized concentration distribution can be given as

$$\frac{c(x,t) - c_0}{c' - c_0} = \frac{1}{2}\left[1 + erf\left(\frac{x}{2(Dt)^{\frac{1}{2}}}\right)\right] \quad (10)$$

If the boundary conditions are just opposite to that described by Equation 5, Equation 10 is then simply changed as

$$\frac{c(x,t) - c_0}{c' - c_0} = \frac{1}{2}\left[1 - erf\left(\frac{x}{2(Dt)^{\frac{1}{2}}}\right)\right] \quad (11)$$

It is noticed that each value of the ratio $[c(x,t) - c_0]/(c' - c_0)$ is associated with a particular dimensionless parameter $x/2(Dt)^{\frac{1}{2}}$. When the $c(x,t)$ is close to c_0, the value of the parameter $x/2(Dt)^{\frac{1}{2}}$ is about 2.80 determined from error function table. The diffusion coefficient D can be determined if the parameters x and t are known. The diffusion coefficients for different ions are presented in Table II. The normalized concentration distributions of the diffusion ions can be numerically simulated by using Equations 10 or 11. The typical result for Ni^{2+} ion in the E–F diffusion couple (diffusion conditions: 1250 °C/4 h) is shown in Fig. 11, in which the EPMA experimental result is also presented for comparison. It is observed

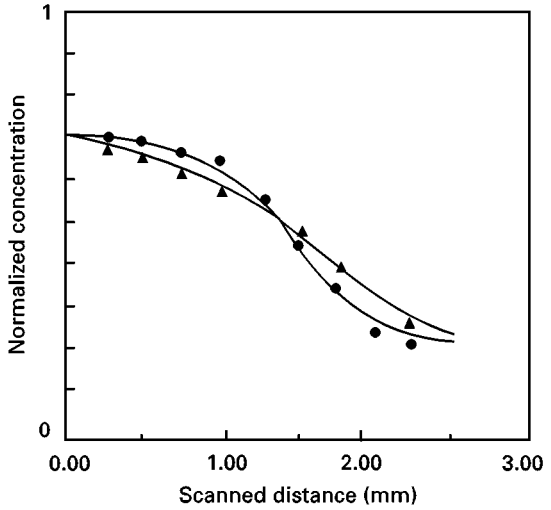

Figure 11 Comparisons between the normalized concentration distribution for Ni^{2+} ion simulated by the computer (▲) and that obtained from the EPMA experiment (●).

that the width of the interdiffusion layer determined by EPMA is wider than that obtained from theoretical simulation. Similar results also occur for other diffusion ions. From an atomic perspective, diffusion in solid materials is just the stepwise migration of atoms from one lattice site to another. In fact, several different ions participate in the diffusion reaction in the PZT/PNN FGM piezoelectric ceramics, and affect each other. Furthermore, there exists several diffusion mechanisms such as the vacancy diffusion and interstitial diffusion, as a consequence, the practical diffusion process is much more complex and slower than that of the theoretical simulation.

4. Conclusions

The interdiffusion reactions between the PZT and PNN phases in the PZT/PNN system FGM piezoelectric ceramics were investigated. The compositional distribution of the interdiffusion region was examined by EPMA and simulated numerically based on a model of overlapping the diffusion solution from thin slab. The diffusion coefficients and activation energies for the diffusion series (Ni^{2+}, Nb^{5+}, Ti^{4+} and Zr^{4+} ions) were determined.

Acknowledgements

The authors are grateful to Professor Xiangting Li, Shanghai Institute of Ceramics, Chinese Academy of Science, for the EPMA experiment and helpful discussion. This project is supported by the National Natural Science Foundation of China, grant number 59282028.

References

1. X. H. ZHU, Q. WANG and Z. Y. MENG, *J. Mater. Sci. Lett.* **14** (1995) 516.
2. X. H. ZHU and Z. Y. MENG, *Sensors & Actuators A: Physical* **48** (1995) 169.
3. K. K. CHAWLA, "Ceramic matrix composites" (Chapman & Hall, London, 1995).
4. X. H. ZHU, PhD thesis, Xi'an Jiaotong University, Xi'an, 1995.

Received 3 May 1996
and accepted 12 September 1997